

Emission spectra and electronic structure of group IIIa monohalide cations

Th. GlenewinkelMeyer, A. Kowalski, B. Müller, Ch. Ottinger, and W. H. Breckenridge

Citation: *The Journal of Chemical Physics* **89**, 7112 (1988); doi: 10.1063/1.455290

View online: <http://dx.doi.org/10.1063/1.455290>

View Table of Contents: <http://scitation.aip.org/content/aip/journal/jcp/89/12?ver=pdfcov>

Published by the [AIP Publishing](#)

Articles you may be interested in

[On the sideband structure of free electron laser emission spectra](#)

Phys. Plasmas **3**, 402 (1996); 10.1063/1.871866

[The electronic structure of the calcium monohalides. A ligand field approach](#)

J. Chem. Phys. **82**, 5023 (1985); 10.1063/1.448676

[The hyperfine structure of the calcium monohalides](#)

J. Chem. Phys. **74**, 5508 (1981); 10.1063/1.440957

[Electronic absorption spectra of molecular cations](#)

J. Chem. Phys. **72**, 2193 (1980); 10.1063/1.439316

[Electronic Spectra and Structure of the Carbonyl Group](#)

J. Chem. Phys. **27**, 429 (1957); 10.1063/1.1743741



Emission spectra and electronic structure of group IIIa monohalide cations

Th. Glenewinkel-Meyer, A. Kowalski,^{a)} B. Müller,^{b)} and Ch. Ottinger

Max-Planck-Institut für Strömungsforschung, Göttingen, Bunsenstr. 10, 3400 Göttingen, Federal Republic of Germany

W. H. Breckenridge

Department of Chemistry, University of Utah, Salt Lake City, Utah 84112

(Received 16 March 1988; accepted 8 September 1988)

Optical spectra of ten AX^+ ions ($A = B, Al, Ga, In; X = F, Cl, Br$) have been observed in the visible and near UV; a total of 18 band systems were newly discovered. The emission was produced by chemiluminescent reactions $A^+ + X_2$ at low (2–10 eV_{CM}) kinetic energy in a beam-gas arrangement. A position-sensitive photon counting detector with large surface area and very low dark count rate was employed, the resolution was mostly 5–50 Å FWHM. Three types of band systems were observed: (1) For all AX^+ combinations except BCl^+ and BBr^+ , a very broad quasicontinuum with undulatory structure appears. On the basis of electronic state correlation arguments, photoelectron data, some *ab initio* calculations and, in one case, a known emission spectrum ($InCl^+$) these band systems were identified as $B^2\Sigma^+ - X^2\Sigma^+$ transitions. It is concluded that the excited state potentials are considerably displaced against the ground state, and their energetics are given. (2) For six species AX^+ , narrow band systems were observed in the 2500 Å region. They could be clearly identified as being due to $C^2\Pi - X^2\Sigma^+$ transitions by means of comparison with the systematics of the analogous $A^2\Pi - X^2\Sigma^+$ transitions of the isoelectronic alkaline earth halides, by the resolved fine structure, and, in the case of AlF^+ , by an *ab initio* calculation. (3) In the $GaCl^+$, $GaBr^+$, and $InBr^+$ spectra, narrow features accompany the $C-X$ transitions. They are attributed to $D^2\Sigma^+ - X^2\Sigma^+$ transitions, analogous to the alkaline earth halide $B^2\Sigma^+ - X^2\Sigma^+$ band systems. Qualitative electronic state correlations are discussed, and the expected dominant configurations in different regions of the AX^+ ground and excited states are given. These are in accord with recent *ab initio* results on AlF^+ .

INTRODUCTION

At the beginning of all modern spectroscopy was the study of alkali atoms.¹ The empirical analysis of their beautifully simple-structured spectra in the second half of the last century paved the way for the development of quantum mechanics. We now know, of course, that the clarity of the alkali spectra derives from the fact that the emission is due to successive excitation of a single electron (in German very appropriately called the "Leuchtelektron"). The spectra of singly ionized alkaline earth atoms were soon found to exhibit a similarly transparent structure.² This was later recognized as a consequence of the fact that group I (alkali) atoms and group IIa (alkaline earth) atomic ions are isoelectronic.

Even among the molecules there is a class which is in many ways comparable to the one-electron atomic systems. These are the alkaline earth monohalides MX where M designates a group IIa atom and X a halogen. The MX molecules again have a single outer shell (valence) electron, and their ground state, for example, is $^2\Sigma^+$, analogous to the 2S alkali atom ground state. The MX electronic spectra are therefore also very well structured, and, not surprisingly, a very large number of electronically excited states has been found (in Ref. 3, 96 of them are listed, for $M = Be$ through Ba and $X = F$ through I).

Isoelectronic with the MX neutral species are the monohalide cations AX^+ of the group IIIa atoms, A . In stark contrast to the situation with MX , however, there is a great paucity of data on the AX^+ systems. This is probably related to the generally harsher conditions required to produce ions, especially in excited states. Under such circumstances, fairly weakly bound molecular species are easily destroyed. At the time the present work was begun, there were no reports at all in the literature on any AX^+ emission spectrum. The only available information on AX^+ excited states was in the form of some photoelectron spectra (PES), in particular, among the species considered here, on BF^+ ,⁴ $InCl^+$, $InBr^+$,^{5,6} and AlF^+ ,⁷ as well as *ab initio* calculations on AlF^+ ⁷ and $AlCl^+$.⁵ Only recently have optical emission spectra of two AX^+ species been observed; the spectrum of $InCl^+$ from a hollow cathode discharge was photographed at high resolution,⁸ and a band system assigned to BBr^+ was observed in a flowing afterglow⁹ at moderate resolution.

In the present work we have used chemiluminescent ion-molecule reactions of the type



to generate electronically excited species AX^{+*} , with $A = B, Al, Ga, In$ and $X = F, Cl, Br$. We were able to observe extensive chemiluminescence spectra in the 2000–6000 Å region for 10 out of the 12 possible combinations AX^+ . They were identified on the basis of the available information from PES, *ab initio* calculations, and particularly a critical review of the spectroscopy of neutral MX . In many cases

^{a)} Alexander von Humboldt Fellow from the Institute of Experimental Physics, University of Gdańsk, Poland.

^{b)} University of Göttingen graduate student; results presented here are part of a Ph.D. thesis.

at least two band systems could be identified, $^2\Sigma^+ - ^2\Sigma^+$ and $^2\Pi - ^2\Sigma^+$. In the latter case the resolved fine structure splitting confirmed the assignment.

An alternative to chemiluminescence as a method to produce AX^+ emission spectra is the direct excitation of the metal halide vapors by electron impact. This technique was, in fact, occasionally used in the present work and did give some additional information ($GaCl^+$, see below). With most species, however, (BCl_3 , BF_3 , $InCl$, $AlCl_3$), electron bombardment produced very complex spectra, abundant with features such as atomic lines, band systems of neutral AX , apparent polyatomic emission features, and spectra from impurities. In contrast, the chemiluminescent spectra were largely free from such "contaminations" and were therefore much easier to interpret.

The method of chemiluminescence has previously also proved very fruitful in the study of the analogous isoelectronic neutral species MX .¹⁰ Here, in addition to spectroscopic data, important dynamical information could be obtained as well. Applying the technique of ion beam chemiluminescence developed in this laboratory to the AX^+ systems is therefore not only a means of producing AX^+ spectra, but promises to be of great value in elucidating the dynamics of $A^+ + X_2$ reactions. Again, a comparison with the behavior of the analogous isoelectronic neutral reactions $M + X_2$ is very instructive.¹¹ Mass spectrometrically, reactions forming AX^+ have been studied very little. In one report¹² $AlCl^+$ was observed as a minor channel in reactions of Al^+ with alkyl halides.

EXPERIMENTAL

The apparatus has been described previously.¹³ It consists basically of an ion source, ion optics and a mass selector magnet, a target gas cell, light collection optics, a monochromator, a photon counting detector, and digital data processing equipment. The ion extraction voltages were 1000 V for B^+ and Al^+ , 600 V for Ga^+ and 300 V for In^+ , limited by the available magnet current. Prior to entering the target gas cell, the ions were decelerated to collision energies ranging from 2 to 10 eV_{CM}. Typical ion currents through the cell were on the order of a few nA. For the present work considerable modifications were made to three components: the ion source, the ion optics, and the detector.

Ion source

The standard "Colutron" source, which is largely constructed of boron nitride, was replaced by an all-metal version, designed in this laboratory. It was found to allow shorter pump-down times, which were previously limited by the degassing of the boron nitride. The anode was made of tungsten, which proved to be corrosion resistant against halogen plasmas. An additional cylindrical mesh electrode surrounds the cathode and is electrically connected to it. It serves to protect the cathode from excessive ion bombardment. B^+ ions were produced from BF_3 gas as in Refs. 14 and 15. Al^+ and Ga^+ were obtained from $AlCl_3$ and $GaCl_3$, respectively. These solids were heated in an external reser-

voir to 100–130 and 40–80 °C, respectively, to produce vapor pressures of ~10 Torr. Via an all-metal needle valve and inlet line, both kept at ~150 °C, the vapor was admitted to the ion source (~200 °C). The precise ion source pressure is not known, but is estimated to be on the order of 0.1 Torr, from comparison with other gases. In^+ was produced from a 1:1 mixture of solid $InCl$ and In metal, placed directly in the ion source. A discharge in Cl_2 was then struck, which, by vaporization of the $InCl$ and/or $In + Cl_2$ reaction, produced a sufficient current of In^+ . In the case of Al^+ , Ga^+ , and In^+ , the original water cooling of the ion source was substituted by forcing air through the cooling coil.

The discharge voltage was in the 50–150 V range. The higher voltages tend to favor the content of metastable 3P state ions in the beam (up to ~20%), which enhances the luminescence yield. The discharge current was ~0.3 A.

Ion optics

A major problem of the original arrangement resulted from operating the ion source with room temperature solids such as $AlCl_3$. The vapor issuing from the anode orifice tends to condense on those ion optics elements which cannot be heated, e.g., the magnet pole faces. For this reason, the ion source axis was in this work positioned perpendicular to the direction towards the magnet, and a 90° electrostatic deflection field was installed in front of the ion source. The electrode arrangement was that of half a hemispherical analyzer of 5 cm radius. Thus, the inner electrode was in the form of a quarter sphere, the outer was a quarter of a hollow sphere, with a 2 cm separation between the two. Both were fabricated out of solid stainless steel blocks, which were kept at 250 °C. This arrangement focuses the beam in two dimensions, and the object and image distances from the respective field boundaries are 5 cm each, with a magnification of unity. The overall transmission is at least 50%. The typical ion current, at full extraction voltage, in the target gas cell was 20–80 nA. The energies typically used to take spectra were between 5 and 30 eV, and the current was then 3–30 nA. The ion beam stability was very good for B^+ , good for Al^+ , and satisfactory for Ga^+ . The In^+ beam intensity, however, fluctuated strongly and rapidly.

Detector

The initial experiments were done with the previously used combination of a photomultiplier, photon-counting electronics, and a 1024 multichannel analyzer. However, the very low light level (a few counts per second, at 26 Å FWHM) and the beam instabilities made it imperative to employ an advanced optical multichannel detection system. With this arrangement, the monochromator exit slit is removed and the spectrum is imaged onto the position-sensitive cathode of a special detector tube. It was necessary to modify the optics of the McPherson 218 monochromator used: The standard 30 cm focal length, aspheric secondary mirror was replaced by a custom-made spherical mirror having $f = 41.5$ cm. This transferred the image plane to a position outside the monochromator housing, accessible to the detector tube. The type used here was a model F 4146 M

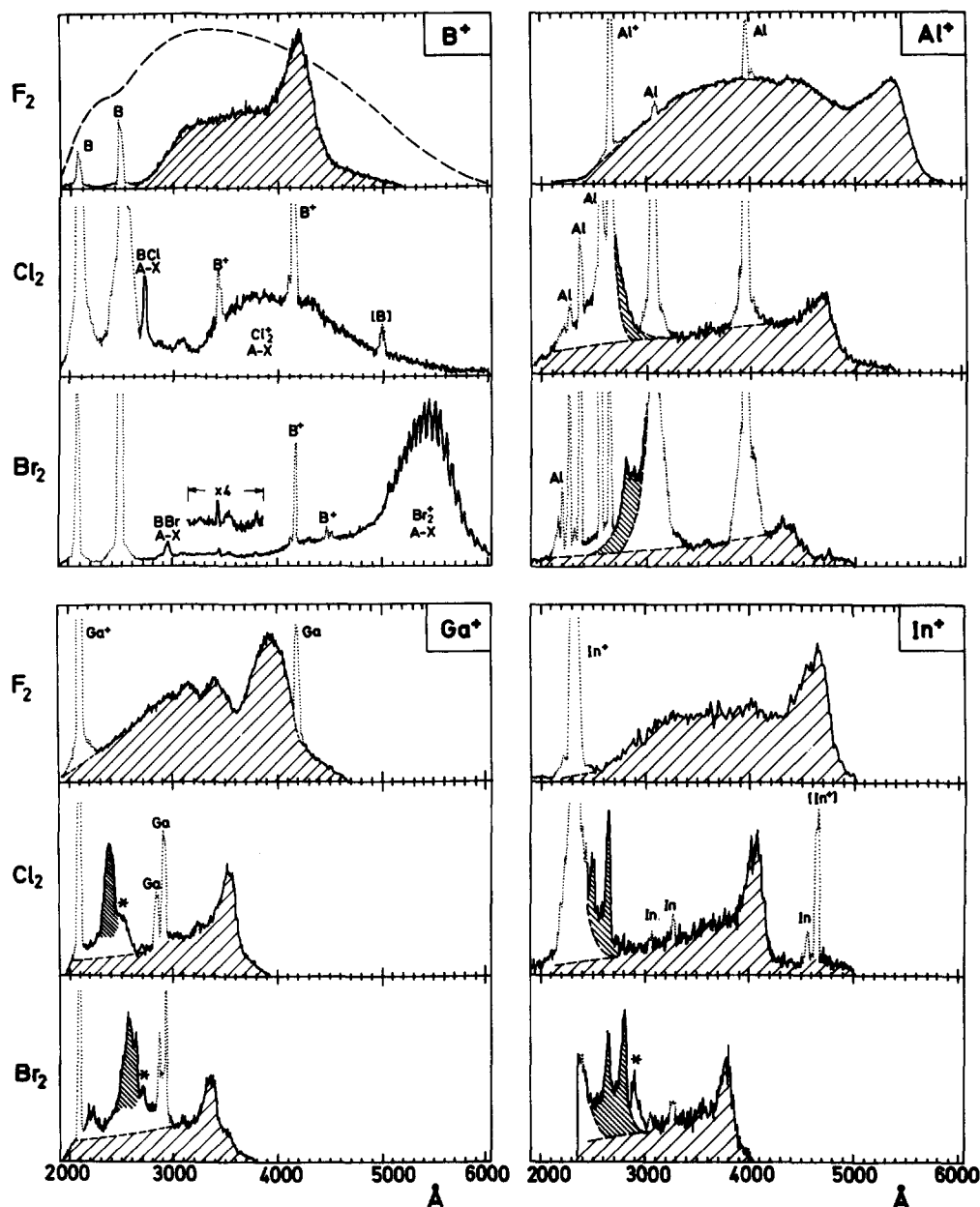


FIG. 1. Chemiluminescence spectra from reactions of four group IIIa atomic ions A^+ ($A = \text{boron through indium}$) with halogens $X_2 = \text{F}_2, \text{Cl}_2, \text{Br}_2$. For collision energies and optical resolution, see Table I. The newly discovered $B^2\Sigma^+ - X^2\Sigma^+$ and $C^2\Pi - X^2\Sigma^+$ band systems of AX^+ are indicated by coarse and fine hatching, respectively. Asterisks mark the suggested $AX^+(D^2\Sigma^+ - X^2\Sigma^+)$ transition. Background atomic lines (dotted) and other known molecular emissions are labeled; [] indicates second order. The dashed curve in the top left panel gives the relative spectral sensitivity curve of the detector, in units of energy/second. In the $\text{In}^+ + \text{F}_2$ and $\text{In}^+ + \text{Br}_2$ spectra, the extreme red end (estimated extent 300–500 Å) was not recorded.

tube, thermoelectrically cooled, in a 2601 Å system, manufactured by ITT/SSL. It incorporates a 25 mm diam bialkali photocathode, a fivefold microchannel plate intensifier and a resistive anode. Four amplifiers, connected to the corners of the anode, deliver charge pulses from each photon event into an analog network, which computes the x/y coordinates of the photon impact on the cathode. The digitized information is stored in a model 2412 A memory, which is divided into 1024×4 channels for the x and y coordinates, respectively. This gives a maximum digital resolution of about 25 μ . The overall actual resolution limit is set by the specified tube resolution of 52 μ plus the aberrations of the monochromator optics, amounting to a total measured FWHM of

$\sim 130 \mu$. The measured dark current was 3.6 counts/s (integrated over the entire cathode area) at -30°C . The system was interfaced with a PDP 11/23 computer which handled the data acquisition and provided online spectrum display.

With a 1200 lines/mm grating, the dispersion is 19 Å/mm, enabling a spectral range 350 Å wide to be covered simultaneously (i.e., with the grating kept at a fixed position). Wider spectra were taken in successive steps, with somewhat overlapping ranges. Alternatively, a 300 lines/mm grating was used which gives an 80 Å/mm dispersion and a 1600 Å coverage per exposure. It can be shown that the gain in total data collection time, compared to the conventional scanning technique is, for 10 Å FWHM resolu-

tion and for a typical signal of 5 counts/s with the conventional technique, about a factor of 140 for both gratings. In this work the coarser grating was mostly used, because it offers the convenience of having to join only two or three spectral sections to cover the full width of the spectra studied (as much as 4000 Å, for AlF⁺). Under these conditions, the total data accumulation times for a complete spectrum were on the order of 1 h.

A further important advantage of the optical multichannel detection scheme is its insensitivity against any signal fluctuations, or indeed a total short-term loss of the ion beam. In this respect, the system time integrates the signal just like a photographic plate does.

A disadvantage, on the other hand, is that the detector tubes are not quite free from "blooming." This term describes the fringe intensity surrounding an isolated, bright spot on the cathode. In our case it appears in the form of a broadening of the base portion of otherwise sharp atomic lines. It affects only the bottom 1%–2%, relative to the peak intensity, but even this can be troublesome if a very intense atomic emission line lies close to a weak feature of interest. However, since the line profile, including blooming, is known, subtraction techniques can help to some extent.

RESULTS AND DISCUSSION

Figure 1 shows a complete survey of spectra, taken with the 12 reaction systems studied. The 300 lines/mm grating was used, and the experimental parameters are collected in Table I. The halogen target gas pressure was usually about 1 Pa (5–10 mTorr). The spectra are not corrected for the relative spectral sensitivity of the monochromator/detector combination, which is shown in the B⁺ + F₂ panel. The ordinate scales of the 12 spectra are not related to each other.

Those portions of the spectra which are due to AX⁺ emission, the primary topic of this paper, are emphasized by hatching and are discussed in the following. The remaining features are atomic lines and some additional molecular band systems as labeled in Fig. 1. Their discussion is deferred to the Appendix.

TABLE I. Group IIIa atomic ion chemiluminescent reactions studied in this work.

Reaction	Collision energy ^a (in eV _{CM})	Resolution ^a (in Å FWHM)
B ⁺ + F ₂	3.9	50
B ⁺ + Cl ₂	4.3	50
B ⁺ + Br ₂	4.7	25
Al ⁺ + F ₂	2.3	40
Al ⁺ + Cl ₂	7.2	40
Al ⁺ + Br ₂	4.3	25
Ga ⁺ + F ₂	10.6	50
Ga ⁺ + Cl ₂	5.1	50
Ga ⁺ + Br ₂	6.9	25
In ⁺ + F ₂	2.5	100
In ⁺ + Cl ₂	3.8	50
In ⁺ + Br ₂	5.8	50

^a Conditions used to take spectra shown in Fig. 1.

TABLE II. Atomic energy levels, relative to A⁺(¹S₀) (in eV).^a

	A	B	Al	Ga	In
Energy A ⁺ (³ P ₀)		4.63	4.63	5.87	5.24
Energy A ⁺ (³ P ₁)		4.63	4.64	5.93	5.37
Energy A ⁺ (³ P ₂)		4.63	4.66	6.04	5.68
Energy A ⁺ (³ P) ^b		4.63	4.65	5.98	5.53
Energy A ⁺⁺ (² S) + X ^{-c}		21.70	15.37	17.12	15.41
Energy A ⁺⁺ (² P) + X ^{-cd}		27.70	22.05	25.34	22.86

^a Atomic energy data from Ref. 17.

^b Weighted mean of fine structure components.

^c For X = F, with electron affinity 3.45 eV; for X = Cl subtract 0.16 eV, for X = Br add 0.09 eV to the energies given (all electron affinities from Ref. 18).

^d The energy of A⁺⁺(²P) is the weighted mean of the ²P_{1/2,3/2} levels.

A thorough literature search showed that none of the shaded areas in Fig. 1 can be attributed to known band systems of emitters composed of the participating atoms, in particular not to AX emissions. Although some of the less common AX band systems do occur within the region where we find emission (e.g., in the case of BF¹⁶), their extent never matches the observation. We therefore ascribe all the shaded features in Fig. 1 to AX⁺ band systems, nearly all of them not hitherto reported.

B²Σ⁺–X²Σ⁺ transitions

The most striking structures in all spectra except B⁺ + Cl₂, Br₂, are those indicated by the coarse shading. They all have in common a rather abrupt rise to a peak at long wavelengths, sometimes preceded by a low "pedestal," and in most cases followed by one or more undulations towards shorter wavelengths. Even at higher resolution (5 Å FWHM), individual bands could not be distinguished. Very characteristic is the monotonic blue shift of the long-wavelength peak in going from F₂ to Cl₂ to Br₂, observed for all projectile ions except B⁺. In each case the change between F₂ and Cl₂ is larger than between Cl₂ and Br₂. These AX⁺ band systems are obviously all related to each other.

Another characteristic trend, again with the exception of B⁺, is the shift of the long-wavelength peak in the sequence Al⁺ → Ga⁺ → In⁺, keeping the halogen fixed. Here we find, after converting the peak wavelength to electron volts and averaging over the three halogens, a shift to the blue by 0.84 eV between Al⁺ and Ga⁺ and back towards the red by about half this amount, –0.44 eV, between Ga⁺ and In⁺. A similar trend of energy differences is found between the corresponding atomic ³P state levels of A⁺: 1.33 eV for Al⁺–Ga⁺, but –0.45 eV, i.e., again in the opposite direction, for Ga⁺–In⁺ (see Table II, which also gives other pertinent atomic energies).

This last observation is a strong clue to the origin of the band systems in question: Their upper states must be closely related to the A⁺(³P) levels. The situation is reminiscent of that with the A⁺ hydrides, e.g., BH⁺ and AlH⁺.^{15,19,20} In those cases covalent A⁺(³P)–H(²S) bonding and A⁺(¹S)–H(²S) repulsion lead to an avoided crossing of two ²Σ potential curves. The resulting adiabatic states are a rather weakly

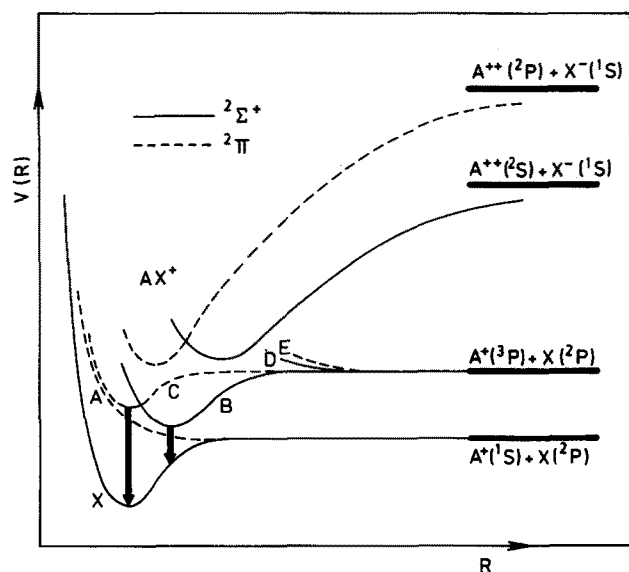


FIG. 2. Schematic potential energy curves of the group IIIa halide ions, AX^+ , and their dissociation limits. The Coulombic correlations shown with the $A^{++} + X^-$ asymptotes are diabatic.

bound $X^2\Sigma$ ground state and an excited $B^2\Sigma$ state, which was first observed in this laboratory.^{14,15,20} The $B^2\Sigma$ potential curve is considerably displaced towards larger internuclear distances, with respect to r_e of the ground state. Consequently, the $B-X$ emission bands of BH^+ ¹⁵ and of AlH^+ ²⁰ were found to span very wide wavelength ranges. The corresponding states in the present case are schematically shown in Fig. 2. The bonding, especially in the ground state, is here strongly modified by ionic contributions, as was first put forward by Berkowitz.^{5,21} This is indicated in Fig. 2 by the Coulombic $^2\Sigma^+$ curve, correlating with $A^{++}(^2S) + X^-$. The AH^+ potentials, too, contain a certain amount of ionic bonding.¹⁹

The analogies with BH^+ and AlH^+ as regards the dissociation asymptotes as well as the similar appearance of the band systems, covering unusually wide wavelength ranges, have led us to assign the newly observed spectra to the $B^2\Sigma^+ - X^2\Sigma^+$ transitions of the various AX^+ species. Strong support of this identification comes from three types of sources: Optical spectroscopy for one of the ten systems in question ($InCl^+$), photoelectron spectroscopy of the GaX and InX compounds, and *ab initio* calculations of AlF^+ .

Some bands of the $B-X$ emission spectrum of $InCl^+$ have recently been observed and unambiguously identified as a $^2\Sigma^+ - ^2\Sigma^+$ transition with the characteristics expected for this system.⁸ In particular, the extrapolated ground state dissociation energy, $D_0(X^2\Sigma^+) = 5800\text{ cm}^{-1}$ or 0.72 eV, agrees very well with that derived from the $InCl$ ionization potential, measured by photoelectron spectroscopy²: $D_0(InCl^+) = D_0(InCl) + IP(In) - IP(InCl) = 4.44\text{ eV} + 5.79\text{ eV} - 9.5\text{ eV} = 0.73\text{ eV}$. Furthermore, the ν_{00} wave number of $26\,989\text{ cm}^{-1} = 3.35\text{ eV}$ agrees with the separation of 3.3 eV between the first ($X^2\Sigma^+$) and the third ($B^2\Sigma^+$) peak in the $InCl$ photoelectron spectrum.⁵ Comparing with the spectrum shown in Fig. 1, the bands identified in⁸ ($v' = 0, v'' = 0-10$, and a few additional $v' = 1$ and 2 bands) lie in the 3616–4162 Å range, thus covering a major

portion of the emission observed by us. For $InBr$, too, the $B-X$ peak separation of 3.3–3.4 eV in the photoelectron spectrum^{5,6} agrees very well with the wavelength of the peak of the $InBr^+$ spectrum ($\sim 3800\text{ Å}$, see Fig. 1).

The separation between adjacent bands in Ref. 8 is about 4.5 Å, comparable to the best resolution used in this work. However, we cannot necessarily expect to resolve individual bands under our conditions; contrary to the thermalized upper state vibrational level population of Ref. 8, ion-chemiluminescence usually yields highly vibrationally and rotationally excited products.¹³ This will produce a quasicontinuum of many broad bands. The characteristic contour of our spectra, exhibiting a peak and a tail to the red, is probably the result of the combined emission from a large number of v' levels, considering, in particular, the expected displacement of the B and X states: The long-wavelength end of the spectrum will result from transitions to high v'' levels, which will be emphasized if the B state is displaced outward. In fact, for a large displacement the transitions will occur into a region where the ground state potential is rather flat. This is the condition for the well-known Condon diffraction bands²²: These are fluctuations of a true emission continuum, which typically join, towards the blue, onto a peak occurring at the red end of the spectrum [which corresponds to transitions at the minimum of the difference potential, e.g., here $V(B) - V(X)$]. The GaF^+ spectrum of Fig. 1, in particular, may be an example of this effect.

The high-resolution optical spectra of $InCl^+$,⁸ very accurate *ab initio* calculations on AlF^+ as well as the available photoelectron spectra give also direct evidence of the postulated shift of the B vs the X state. In Ref. 8, the long v'' progression observed as well as the pronounced red degradation of the bands confirm a displacement of the B state [by $\sim 10\%$ of $r_e(X)$]. For AlF^+ , high-quality calculations of potentials have very recently been done,²³ which give r_e values of 1.60 and 2.17 Å for the $X^2\Sigma^+$ and $B^2\Sigma^+$ states, respectively. Finally, in the photoelectron spectra of InF ,²⁴ $InCl$, and $InBr$,^{5,6} the width of the $B^2\Sigma^+$ peak and that of the $X^2\Sigma^+$ peak give an indication of the displacements of these potentials, both relative to the AX ground state interatomic distance. It turns out that the $X^2\Sigma^+$ peaks of InF , $InCl$, and $InBr$ are all quite narrow (0.20, 0.21, 0.16 eV FWHM, respectively), indicating that the interatomic distance of the AX^+ ground state increases in going from F to Cl to Br by about as much as does that of the AX ground state.³ The $B^2\Sigma^+$ peaks of InF , $InCl$, and $InBr$, on the other hand, are all much broader, but decrease characteristically in width in the above order: 0.51, 0.46, 0.32 eV FWHM. Obviously, the large (outward) displacement of $B^2\Sigma^+$, relative to $X^2\Sigma^+$, for the fluoride (cf. the *ab initio* results for AlF^+) diminishes in going to the bromide; therefore, on an absolute radial scale the $B^2\Sigma^+$ potential well shifts less towards larger r than do both the $X^2\Sigma^+$ and the neutral compound $X^1\Sigma^+$ ground states.

This result is quite plausible: Both of the latter states are distinctly ionic in character⁵ and will therefore, through the ion-induced dipole term, respond strongly to the polarizabilities α of X^- . The Coulombic plus ion-induced dipole potential is

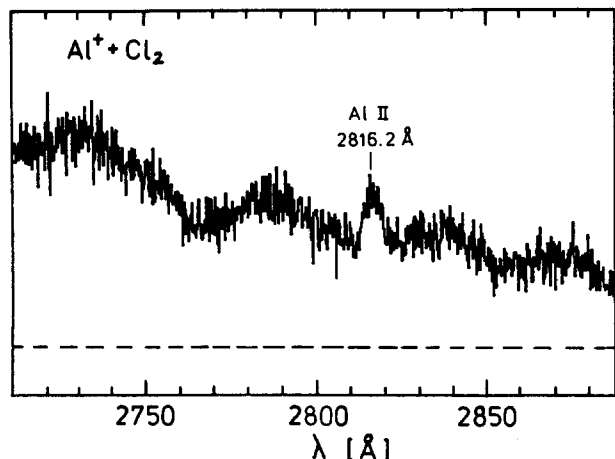


FIG. 3. Portion of the spectrum from $\text{Al}^+ + \text{Cl}_2$ collisions, taken at a resolution of 7 \AA FWHM (collision energy $7.3 \text{ eV}_{\text{CM}}$). A weak background Al^+ emission line is indicated. The dashed line gives the detector dark current.

$$V(r) = \frac{-q_1 q_2}{r} - \frac{1}{2} \frac{q_1^2 \alpha_2}{r^4}, \quad (2)$$

where $\alpha_2 = 2.24,^{25} 5.6,^{26}$ and 6.5 \AA^3 ²⁷ for F^- , Cl^- , and Br^- , respectively.

Assuming a pure $\text{A}^+ + \text{X}^-$ configuration of the AX^+ ground state, the contribution of the second potential term, at a characteristic internuclear distance of 2.3 \AA , amounts to as much as $-2.3, -5.8, -6.7 \text{ eV}$ for $\text{X} = \text{F}, \text{Cl}, \text{Br}$. The corresponding radial changes (compared to a pure Coulomb potential) are $\Delta r = +0.4, +0.7, +0.8 \text{ \AA}$. The effect on r of the AX ground state, assumed as $\text{A}^+ \text{X}^-$, is calculated to

be about half this amount. The $B^2\Sigma^+$ state of AX^+ , however, is much less ionic than the AX^+ ground state and will therefore change its radial position less, as X is varied. This is in agreement with the conclusion drawn from the photoelectron spectra.

On this basis we can now also explain the characteristic blue shift of the $B\text{-X}$ spectra which appears so strikingly in Fig. 1. For the fluorides, with their large relative $B^2\Sigma^+ - X^2\Sigma^+$ radial displacement, the bulk of the $B\text{-X}$ emission will occur to the right limb of the groundstate potential well, i.e., into rather high v'' levels. In going to the chlorides and bromides, however, the X state potential moves more "under" the B state, so that radiative transitions will now occur largely close to the $X^2\Sigma^+$ potential minimum. Accordingly, the emission will shift towards shorter wavelengths.

The somewhat irregular trend of this blue shift further supports this explanation: Figure 1 shows clearly that it is much larger between AF^+ and ACl^+ than between ACl^+ and ABr^+ , for the three metals $\text{A} = \text{Al}^+, \text{Ga}^+, \text{In}^+$. This correlates nicely with the unequal increments in the polarizability of X^- and hence the predicted outward shifts of the $X^2\Sigma^+$ potentials.

Table III summarizes the energetics of the $B^2\Sigma^+$ potentials of AX^+ ions, as derived from this work. λ_{max} gives an upper limit to the energy E_{min} of the B state potential at the $v' = 0$ level, relative to the $\text{A}^+ (^1S) + \text{X}$ dissociation asymptote, see Fig. 2. Literature data of ionization potentials $\text{IP}(\text{AX})$ are included in Table III to enable the ground state dissociation energies $D_0(\text{AX}^+)$ to be evaluated (where not otherwise known). $T_0(B^2\Sigma^+)$ refers the $v' = 0$ level of the B states to the ground state $v'' = 0$ levels. The B state dissocia-

TABLE III. Summary of data on the $B^2\Sigma^+$ states of AX^+ .

AX^+	λ_{max}^a (\AA)	E_{min}^b (eV)	$\text{IP}(\text{AX})$ (eV)	$D_0^c(\text{AX}^+)$ (eV)	$T_0(B^2\Sigma^+)^c$ (eV)	$D_0(B^2\Sigma^+)^d$ (eV)	$\Delta E[\text{AX}^+(B)]^e$ (eV)
BF^+	5200	2.4	11.115 ^f	5.0 ^g	7.4	2.2	-0.6
AlF^+	5900	2.1	9.8 ^h	3.1 ⁱ	5.2 ^j	2.6	-1.2
AlCl^+	5400	2.3		1.4 ^k	3.7	2.4	+0.2
AlBr^+	5000	2.5				2.2	
GaF^+	4700	2.6	10.7 ^l	1.3 ^g	3.9	3.4	-1.8
GaCl^+	3900	3.2	10.04 ^l	0.9 ^g	4.1	2.8	-0.3
GaBr^+	3800	3.3	9.84 ^l	0.5 ^g	3.8	2.7	-0.7
InF^+	5000 ^m	2.5	9.95 ^l	1.1 ^g	3.6	3.0	-1.3
InCl^+	5000	2.5	9.61 ⁿ	0.72 ^o	3.2 ^p	3.0	-0.4
InBr^+	4100 ^m	3.0	9.22 ^q	0.56 ^g	3.6 ^p	2.5	-0.4

^a Long-wavelength limit of $B^2\Sigma^+ - X^2\Sigma^+$ band systems observed in this work.

^b $E_{\text{min}} = hc/\lambda_{\text{max}}$ is taken to be the energy of the $\text{AX}^+(B^2\Sigma^+)$ potential minimum relative to the $\text{A}^+ (^1S) + \text{X}$ energy level.

^c $T_0(B^2\Sigma^+) = D_0^c(\text{AX}^+) + E_{\text{min}}$ is the B state energy relative to bound $\text{AX}^+(X^2\Sigma^+) v = 0$.

^d $D_0(B) = E(^3P) - E_{\text{min}}$; for values of $E(^3P)$ see Table II.

^e Energy balance of the reaction $\text{A}^+ (^3P) + \text{X}_2 \rightarrow \text{AX}^+(B^2\Sigma^+) + \text{X}$ (negative sign for exothermic reaction).

^f Reference 3.

^g Calculated as $D_0(\text{AX}) + \text{IP}(\text{A}) - \text{IP}(\text{AX})$, where $D_0(\text{AX})$ was taken from Ref. 3 and $\text{IP}(\text{A})$ from Ref. 18.

^h Reference 7.

ⁱ Reference 23.

^j The *ab initio* work gives 4.9 eV (Ref. 23).

^k Reference 5.

^l Reference 24.

^m For experimental reasons the extreme red end of the spectra was not observed.

ⁿ Average of 9.51 eV (Ref. 5) and 9.71 eV (Ref. 6).

^o Reference 8.

^p Reference 3 gives 3.3 eV .

^q Average of 9.09 eV (Ref. 5) and 9.35 eV (Ref. 6).

tion energies $D_0(B^2\Sigma^+)$ were calculated from $D_0(B) = E(^3P) - E_{\min}$, where $E(^3P)$ is the energy of $A^+(^3P)$ (Table II). The last column of Table III gives the exothermicities of the chemiluminescence reactions used to produce the $AX^+(B)$ species, starting from A^+ in the 3P state. It has been shown that $A^+(^3P)$ is in fact the dominant reactant ion species.¹¹ Unlike most of the chemiluminescent ion-molecule reactions studied previously in this laboratory, all reactions listed here are exothermic or practically thermoneutral.

In conclusion of this discussion of the $AX^+ B^2\Sigma^+ - X^2\Sigma^+$ transitions, we wish to emphasize that these are *not* the analog of the lowest $^2\Sigma^- - ^2\Sigma$ transition of the isoelectronic MX species, which are traditionally also designated by the symbols $B-X$. These latter ones are entirely different both in appearance of the spectra and in their structural origin. The $MX B-X$ spectra are confined to rather narrow spectral regions, close to the similarly compact $A^2\Pi-X^2\Sigma^+$ spectra. As will be discussed below for the corresponding AX^+ species, both the A and B states of MX are strongly ionic, correlating diabatically with excited M^+ . Their potential minima lie at a comparatively small internuclear distance. The $AX^+ B^2\Sigma^+$ states, by contrast, were shown to be much less ionic in character, correlating with the analog of neutral $M(^3P)$, and having potential minima which are at a large internuclear separation. The question arises, then, why no spectra of MX have been reported which would truly correspond to the $AX^+ B-X$ transitions. From the correlation rules, an analogous $^2\Sigma^+$ state must certainly arise from $M(^3P) + X(^2P)$. It is likely, however, that it is not bound. Considering the much smaller $^3P-^1S$ energy gap for M atoms (typically 1.8–2.7 eV) in comparison to A^+ ions (4.6–6.0 eV), the interaction of the two covalent $^2\Sigma^+$ states arising from the 1S and 3P asymptotes will be much stronger in the MX case. Their mutual repulsion may then well eliminate the bonding in the upper $^2\Sigma^+$ state.

$C^2\Pi-X^2\Sigma^+$ transitions

Besides the broad $AX^+(B-X)$ quasicontinuum, the other major feature of interest appearing in many of the spectra of Fig. 1 is an intense, but narrow band system. It is concentrated near 2500 Å and is emphasized in Fig. 1 by narrow hatching. For the Ga^+ and In^+ reactions, this emission feature is very distinct, while with Al^+ it is blended with the bases of intense Al^+ and Al lines (see Appendix) and can only be clearly identified after subtraction of this line profile. Spectra taken at higher resolution, however, show a regular band structure even in the difficult $AlCl^+$ case, see Fig. 3. The shaded area near 2700–2900 Å in the $Al^+ + Br_2$ spectrum also requires caution in the interpretation. It may be due, in part, to the known $A^1\Pi-X^1\Sigma^+$ transition of $AlBr$,³ which might be formed in this reaction (see Appendix). However, high-resolution spectra and a consideration of the $AlBr$ Franck-Condon factor distribution show again that certainly not all of the emission can be attributed to $AlBr$ (if any; the corresponding $AlCl$ emission might then also be expected, but is clearly absent at 2615 Å).

The characteristic doublet splitting which is observed in the $InCl^+$ and $InBr^+$ cases was also investigated at higher

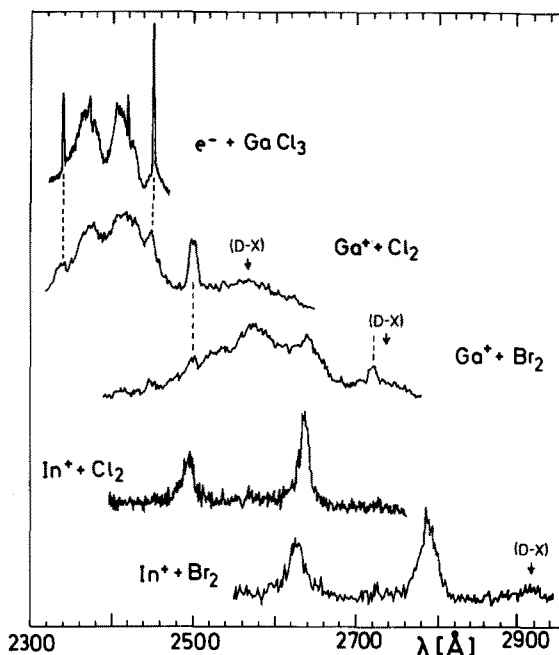


FIG. 4. $C^2\Pi-X^2\Sigma^+$ chemiluminescence spectra of $GaCl^+$, $GaBr^+$, $InCl^+$, $InBr^+$ taken at higher resolution (13 Å FWHM, except 7 Å for $In^+ + Cl_2$), collision energies ~ 5 eV_{CM}. The suggested $D^2\Sigma^+ - X^2\Sigma^+$ emissions are indicated by arrows. A $GaCl^+(C-X)$ spectrum obtained from collisions of 820 eV electrons with $GaCl_3$ has been included (top, 1.7 Å FWHM). Underlying atomic emissions are marked by dashed lines.

resolution, see Fig. 4. Here it can be determined with good precision and is quite similar for $InCl^+$ and $InBr^+$ (for numerical results, see Table VII below). The $Ga^+ + Cl_2$ and $Ga^+ + Br_2$ spectra also show a structure consisting of two rather broad peaks. Due to the greater width of the two components compared to the In^+ reactions, their smaller separation, and the low chemiluminescence intensity, the splitting could here not be measured as accurately. However, for $GaCl^+$, improved data were obtained from an auxiliary experiment in which $GaCl_3$ vapor was directly admitted to the observation region and bombarded with electrons (simply using the ion source filament as a source, with reversed extraction voltage and magnet current). The resulting spectrum is shown in Fig. 4, top. It is very similar, as regards the doublet structure, to the adjacent $Ga^+ + Cl_2$ chemiluminescence spectrum. This is additional evidence that this feature is indeed due to $GaCl^+$. For the $Ga^+ + Br_2$ case a comparable splitting can be read from the spectrum in Fig. 4, middle. This parallels the similarity of the $In^+ + Cl_2, Br_2$ splittings.

We conclude this summary of the observations with the remark that any corresponding spectral feature is completely absent in all four $A^+ + F_2$ reactions. The spectra taken with fluorine are particularly clean, due to the high ionization potential of F_2 which largely inhibits any luminescent charge transfer. The striking nonexistence (in the 2000–6000 Å range) of the band systems in question is therefore very well documented.

The identification and interpretation of these electronic transitions rests squarely on analogies with the corresponding isoelectronic MX systems. Here the best-known spectra

TABLE IV. Energy T_e (in eV) of $\text{MX}(A^2\Pi, X^2\Sigma^+)$ transitions.^a

M \ X	F	Cl	Br	I	$\langle T_e \rangle$					
Be	4.12	3.47	3.27	3.29	2.92	2.96	3.41			
Mg	3.45	3.45	3.28	3.29	3.19	3.21	3.02	3.24	3.24	
Ca	2.04	2.05	2.00	2.00	1.97	1.98	1.93	1.94	1.99	1.99
Sr	1.87	1.90	1.84	1.87	1.82	1.86	1.79	1.83	1.83	1.87
Ba	1.44	1.52	1.28	1.36	1.24	1.31	1.15	1.23	1.28	1.36

^aThe first entry in each column refers to $^2\Pi_{1/2}$, the second to $^2\Pi_{3/2}$. All values taken from Ref. 3.

are due to the $A^2\Pi-X^2\Sigma^+$ and the $B^2\Sigma^+-X^2\Sigma^+$ transitions. Similar to the AX emission features at hand, they cover rather narrow wavelength ranges, the A-X spectrum lying close to the B-X bands on the "red" side. Thus, the lowest known excited state of all 20 MX species ($M = \text{Be}-\text{Ba}$, $X = \text{F}-\text{I}$) is the $A^2\Pi$. This led us to associate, tentatively at first, the newly observed AX^+ bands with the analogous $^2\Pi-X^2\Sigma^+$ transition. For the AX^+ species, this postulated bound $^2\Pi$ state must be designated as $C^2\Pi$, because the lowest lying excited state, $A^2\Pi_i$, is here repulsive. It has been observed in the photoelectron spectra of some AX molecules^{5,6,21,24} as a very wide peak lying between the sharp $X^2\Sigma^+$ and the broader $B^2\Sigma^+$ peak. No $C^2\Pi$ state has ever been reported in the photoelectron spectra of any AX species. *Ab initio* calculations for AlCl^+ and AlF^+ do show a bound $^2\Pi_r$ state.²³

The key to a quantitative identification of the AX^+ $C^2\Pi_r$ states is furnished by a comparative review of the known spectroscopic data of the MX molecules and the M^+ ions.

The term energies T_e of the 20 MX $A^2\Pi_{1/2,3/2}$ states, from Ref. 3, are collected in Table IV. It is seen that they depend strongly on the metal M, but much less on the halogen X. The last column gives, therefore, the X-averaged term values, $\langle T_e \rangle$. Table V gives on the left the energies of the resonance $^2P_{1/2,3/2}$ levels, E_{res} , of the alkali-like M^+ ions, taken from Ref. 17. A very interesting correlation can be seen between the $\langle T_e \rangle$ and these E_{res} values, which is graphically presented in the left half of Fig. 5. It demonstrates vividly the fact that the A states of MX derive, according to their wave function composition, largely from the dissociation products $M^+(^2P) + X^-$. The MX ground states, on the other hand, correlate with ground state $M^+(^2S) + X^-$. Thus, the asymptotic excitation energy E_{res} of the metal ion carries over, with some modification by the binding to the

TABLE V. Energies of 2P atomic resonance levels.

M^+	E_{res} (eV)		A^{++}	E_{res} (eV)	
	$^2P_{1/2}$	$^2P_{3/2}$		$^2P_{1/2}$	$^2P_{3/2}$
Be ⁺	3.96	3.96	B ⁺⁺	5.99	6.00
Mg ⁺	4.42	4.42	Al ⁺⁺	6.65	6.68
Ca ⁺	3.12	3.15 ^a	Ga ⁺⁺	8.08	8.29
Sr ⁺	2.94	3.04 ^a	In ⁺⁺	7.09	7.63
Ba ⁺	2.51	2.72 ^a	Tl ⁺⁺	7.95	9.79

^aThe lowest excited state is 2D (see Ref. 28). All values taken from Ref. 17.

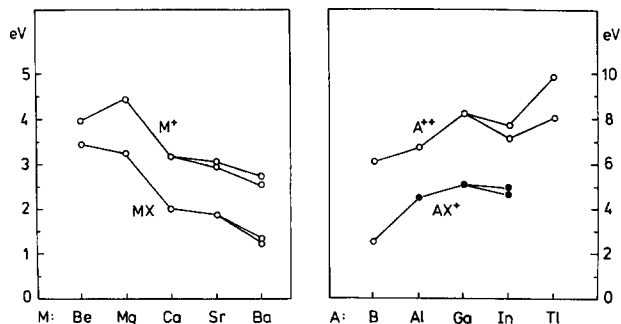


FIG. 5. Left: Comparison of the alkaline earth ion $M^+(^2P)$ resonance energies (E_{res} , see Table V), with the electronic term energies of the corresponding $\text{MX}(A^2\Pi)$ halides ($\langle T_e \rangle$, averaged over $X = \text{F}, \text{Cl}, \text{Br}, \text{I}$, see Table IV). Energies in eV on the left-hand ordinate. Right: The analogous comparison for the respective isoelectronic species: the group IIIa doubly charged ion $A^{++}(^2P)$ resonance energies (Table V) with the $\text{AX}^+(C^2\Pi)$ energies ($\langle T_e \rangle$, averaged over $X = \text{Cl}, \text{Br}$, see Table VI), derived in this work (dots). The AX^+ open circle is from Ref. 9. Note the change of the energy scale on the right-hand side. Pairs of points represent the $^2P_{1/2}-^2P_{3/2}$ atomic (M^+, A^{++}) and $^2\Pi_{1/2}-^2\Pi_{3/2}$ molecular (MX, AX^+) fine-structure splitting. The correlations illustrated here identify the newly discovered $\text{AX}^+(C-X)$ band systems (see the text).

halogen, into the molecular $\text{MX}A^2\Pi$ energy. In this simplified picture the A state is the molecular analog of the atomic M^+ resonance state, underlining again the quasilkali nature of the MX species.

Remembering that AX^+ ions, too, should have quasilkali character, we can expect a similar correlation between the molecular AX^+ excitation energies on the one hand and the 2P resonance levels of the alkali-like A^{++} ions (the isoelectronic counterparts of the M^+ species) on the other. The latter, taken from Ref. 17, are given in the right-half of Table V. The former energies are derived from the peak wavelengths of the spectral features observed in this work. They are tabulated in Table VI. Like in the MX case, they are seen to depend very little on the X species and are therefore given as averaged $\langle T_e \rangle$ in the last column of the table. For BBr^+ , where we have not observed a corresponding emission, data from a reported $\Pi-\Sigma$ transition (Ref. 9, see discussion below) have been included. Figure 5 gives on the right a

TABLE VI. Peak wavelengths and transition energies (in eV) of the $\text{AX}^+(C^2\Pi_{11}-X^2\Sigma^+)$ band system.^a

A \ X	Cl	Br	$\langle T_e \rangle^d$
B	b	2.50 ^c 2.54 ^c	2.50 2.54
Al	2780 Å ^c 4.46	2850 Å ^c 4.35	4.41
Ga	2411 Å 2367 Å 5.13 5.23	2635 Å 2575 Å 4.70 4.81	4.92 5.02
In	2636 Å 2493 Å 4.70 4.97	2787 Å 2625 Å 4.45 4.72	4.58 4.85

^aThe first entry for each AX^+ system is for $\Omega = 1/2$, second entry for $\Omega = 3/2$.

^bNot observed.

^cFrom Ref. 9.

^dAveraged over the halogen X separately for each doublet component.

^eDoublet components not resolved.

TABLE VII. Atomic and molecular fine structure splittings.^a

M		Ca	Sr	A		Ga	In
	MX	X = F	73	281	AX ⁺	X = F	...
		Cl	70	294		Cl	790 ± 80
		Br	63	301	C(2Π _{3/2} -2Π _{1/2})	Br	880 ± 80
(I)		Avg:	69	292		Avg:	835 ± 80
(II)	M ⁺		223	800	A ⁺⁺		1718
							4342
(I) : (II)	2P _{3/2} -2P _{1/2}		0.31	0.37	2P _{3/2} -2P _{1/2}		0.49 ± 0.05
							0.51 ± 0.02

^aAll data except last line in cm⁻¹. Atomic data taken from Ref. 17, molecular data from Ref. 3.

graphical comparison of the average AX⁺ excitation energies $\langle T_e \rangle$ with the A⁺⁺ resonance energies. Again, a close correlation can be noted between the two. Paralleled with the systematics of the MX and M⁺ term energies, this correlation proves that the AX⁺ molecular states in question dissociate diabatically into A⁺⁺(²P) + X⁻. The Coulombic potential curve originating from this asymptote is schematically shown in Fig. 2. Thus, the excited AX⁺ states observed in this work are of an ionic A⁺⁺X⁻ character, just like the AX⁺ ground states. While the latter dissociate to ground state A⁺⁺(²S) ions, the former dissociate diabatically to give excited A⁺⁺(²P).³⁰

However, this description of the excited states of AX⁺ is not sufficient to identify them uniquely as ²Π. Since from the A⁺⁺(²P) + X⁻ asymptote both a ²Π and a ²Σ⁺ state originate, the same argument can be put forward to explain an excited ²Σ⁺ state. In fact, for the MX species the well-known B²Σ state is precisely of this nature. The AX⁺ emission features being discussed here, however, can be definitely assigned to a ²Π-²Σ⁺ transition on account of the resolved ²Π_{1/2}-²Π_{3/2} fine structure splitting in the Ga and In cases (and then also for Al on the basis of the energy correlation shown in Fig. 5, despite the unobservably small splitting in this case).

Again, recourse to the isoelectronic analogs MX allows a quantitative discussion of the fine structure splittings. Table VII lists on the left-hand side the ²Π_{3/2}-²Π_{1/2} term separations for three Ca and Sr halides MX (X = F, Cl, Br), taken from Ref. 3. It is seen that they depend very little on the X atom, similar to the ²Π energies themselves (Table IV). The atomic fine structure splitting M⁺(²P_{1/2,3/2}) is also given. The last line of Table VII shows that, for the MX compounds, the MX(²Π) and M⁺(²P) spin-orbit splittings are about in the ratio 1:3, for both Ca and Sr. In the right-half of the table, analogous data are given for the isoelectronic AX⁺ and A⁺⁺ species. The GaCl⁺, GaBr⁺, InCl⁺, InBr⁺ doublet splittings were read from the spectra shown in Fig. 4, and are again nearly the same for X = Cl, Br. They amount, in this case, to about one-half of the A⁺⁺(²P) spin-orbit splittings (taken from Ref. 17), again for both metals nearly the same fraction. Overall, Table VII demonstrates a great similarity of the MX and AX⁺ fine structure, both as regards the insensitivity against X and the smaller splitting, compared to the dissociated product. This proves beyond any doubt that the newly discovered, narrow band systems,

indicated by close hatching in Fig. 1, are due to the AX⁺(C²Π-X²Σ⁺) transitions.

The dissociation energies of the C²Π states can be calculated according to $D_0(C^2\Pi) = E(^3P) + D_0(AX^+) - T_0(C^2\Pi)$, analogous to the B²Σ⁺ states. Using for T₀ the weighted means of the ²Π_{1/2,3/2} states given in Table VI, the following values are obtained: 1.6, 1.7, 1.7, 1.4, 1.5 eV for AlCl⁺, GaCl⁺, GaBr⁺, InCl⁺, InBr⁺, respectively. The energy balances ΔE[AX⁺(C)] of the reactions A⁺(³P) + X₂ → AX⁺(C) + X can be found from ΔE[AX⁺(B)] given in Table III by adding the term differences T₀(C)-T₀(B). In contrast to the B²Σ⁺ states, formation of AX⁺(C²Π) is endothermic, by 0.5–1.0 eV.

Very conspicuous is the complete absence of any corresponding C → X emission feature in the four fluoride spectra. This is probably due to a predissociation of the attractive C²Π_i state by the repulsive A²Π_i state (cf. Fig. 2). In the case of Al⁺, this hypothesis can be supported quantitatively. Considering Table VI, the expected excitation energy of the AlF⁺ C²Π state would be about 4.5 eV, similar to the measured energies for AlCl⁺ and AlBr⁺; its potential minimum should lie at an internuclear distance close to the r_e of the AlF⁺ ground state. However, the *ab initio* calculations on AlF⁺ show that at this r_e (1.6 Å) the A²Π_i state has an energy of ~5.0 eV, so that it would intersect the C²Π_i potential curve. A strong perturbation, leading to effective predissociation of the C state, is then to be expected. While in Ref. 7 the C state itself was not calculated, very recent theoretical work, which does include it, shows the C/A intersection directly.²³ For AlCl⁺, in comparison, the situation is quite different. Here the available *ab initio* calculations⁵ show the A state to lie much lower, about 3.5 eV above the ground state at its minimum. The C state at 4.5 eV is then sufficiently far above the A state to not be predissociated.

A similar drop in the A-X separation between the fluoride and the chloride obtains also for the Ga and In compounds. Here *ab initio* calculations have not been made, but instead photoelectron spectra are available. They show the repulsive A state to lie at 3.0; 1.3; 0.9 eV above the X state for GaF⁺, GaCl⁺, GaBr⁺, respectively,²⁴ and at 2.3,²⁴ 0.7, 0.6 eV⁵ for InF⁺, InCl⁺, InBr⁺. These relative energies reflect the considerably greater dissociation energies of the X²Σ fluorides compared to the chlorides and bromides—a trend which is also found with the neutral MF vs MCl, MBr species.³ However, the expected GaF⁺ and InF⁺ C → X transi-

tion energies of ~ 5 eV (Table VI) exceed the $A-X$ energy separation considerably, so that on this basis alone a strong predissociation, like in the AlF^+ case, would not be expected. For these two systems more detailed information on the shape of the $A^2\Pi$ state, especially high up on its repulsive wall, is required to verify whether here, too, nonradiative transitions into the A state continuum (predissociation) are responsible for the absence of any $C \rightarrow X$ emission.

It is interesting to make again a comparison with the potentials of the isoelectronic MX species, where the bound $^2\Pi_r$ state (the A state, in the usual notation) lies well *within* the ground state potential and correlates adiabatically with *ground* state products $\text{M}(^1S) + \text{X}(^2P)$, quite different from the situation shown in Fig. 2. This can be rationalized as follows: First of all, the ground state dissociation energy of MX is usually much greater than that of the corresponding AX^+ , so that the ground state potential well can easily “accommodate” a higher state such as the $^2\Pi_r$. For example, $D_0(\text{SrF}) = 5.6$ eV, but $D_0(\text{InF}^+) = 1.1$ eV. This difference is largely due to the fact that the $\text{M}^+(^2S) + \text{X}^-$ asymptote of the Coulombic potential is much lower than the $\text{A}^{++}(^2S) + \text{X}^-$ asymptote, allowing a much greater Coulombic bond strength at a typical radius. As for the excited states, the $\text{M}^+(^2P)$ resonance energies are, on the average, also only half as large as those of $\text{A}^{++}(^2P)$ (Fig. 5). The corresponding excited MX Coulomb potential drops therefore much more deeply than its AX^+ counterpart shown in Fig. 2. Whereas the latter reaches a minimum at the bottom of the $C^2\Pi$ state well, the former will penetrate deeply into the ground state potential. Thus it intersects, for MX, the repulsive $^2\Pi_r$ state. The resulting avoided crossing gives then finally the well-known bound $A^2\Pi_r$ state of MX with ionic character, which, however, connects adiabatically with the $^2\Pi_r$ state and ultimately its $\text{M} + \text{X}$ asymptote. Thus, the same $^2\Pi_r/{}^2\Pi_r$ interaction which we have postulated to manifest itself in the C state predissociation of the AF^+ species has, in the MX molecules, the dramatic consequence of interchanging the ordering and the adiabatic correlations of the two $^2\Pi$ states.

We conclude the discussion of the $\text{AX}^+ {}^2\Pi_r$ states with comments on two experimental results. First, spectroscopic observation of a $\text{BBr}^+({}^2\Pi_r - {}^2\Sigma^+)$ transition has recently been reported⁹ (the upper state is in Ref. 9 labeled $A^2\Pi_r$, not to be confused with the conventional designation of $A^2\Pi_r$ for the repulsive state, as used in this work). A resolved doublet structure was, by analogy with isovalent systems, attributed to a $^2\Pi_r$ upper state. However, referring to Fig. 1, the $C^2\Pi_r - X^2\Sigma^+$ transitions, where identified, are in all cases well to the short-wavelength side of the peaks of the $B-X$ emissions. Considering the progressive blue shift of the latter in the order $\text{X} = \text{F}, \text{Cl}, \text{Br}$, [the small peak appearing in the $\text{B}^+ + \text{Br}_2$ spectrum at 3500 Å may in fact be due to $\text{BBr}^+(B-X)$], the $\text{BBr}^+(C-X)$ transition would then be expected to lie at 3000 Å or less, while the wavelength range reported in Ref. 9 is 4700–5150 Å, with a T_e of 2.50 eV. Now it is noteworthy that among the 12 AX^+ systems considered here, BBr^+ has an exceptional ordering of low-lying asymptotes: Between the $\text{B}^+(^1S) + \text{Br}$ level and the $\text{B}^+(^3P) + \text{Br}$ limit at 4.63 eV (cf. Fig. 2) there is in this case the

$\text{B}(^2P) + \text{Br}^+(^3P_2)$ energy of 3.54 eV. Any $^2\Pi$ state arising from this asymptote would then emit much further in the long-wavelength region than the “typical” $C^2\Pi$ state according to Fig. 2. In fact, from the vibrational analysis given in Ref. 9, the dissociation energies of the two states involved can be calculated from the approximate formula $D_e = \omega_e^2 / 4\omega_e x_e$. One obtains $D'_e = (2.73 \pm 0.14)$ eV, $D''_e = (2.85 \pm 0.18)$ eV, which predicts $T_e = (3.54 + 2.85 - 2.73)$ eV = 3.66 eV. This is still hardly compatible with $T_e = 2.50$ as given in Ref. 9. An alternative interpretation of this emission, if it is indeed due to BBr^+ , is a transition not into the ground state, but connecting two excited states.

It is very unfortunate that in our own spectra the overwhelming Br_2^+ emission (Fig. 1) precludes any observation of the $\text{BBr}^+(C-X)$ system.

The other pertinent experimental observation is a very sharp peak in the AlF photoelectron spectrum, reported by Dyke *et al.*⁷ 5.6 eV above the $X^2\Sigma^+$ ground state. It was tentatively assigned to a shake-up transition to a higher $^2\Sigma^+$ state. However, very recent highly accurate *ab initio* calculations on AlF^{+23} have clearly identified the bound $C^2\Pi_r$ state (not included in the earlier calculations⁷). It agrees precisely with the photoelectron spectrum, both as regards the peak position (the calculated $^2\Pi_r$ energy is 5.60 eV) and the extremely sharp peak profile [the calculated equilibrium $\text{AlF}^+(C)$ distance is 1.678 Å, very similar to $r_e(\text{AlF}) = 1.654$ Å]. Thus, the original assignment of this peak is most likely in error, and it represents, in fact, the first observation of any $\text{AX}^+ C^2\Pi_r$ state.

$D^2\Sigma^+ - X^2\Sigma^+$ transitions

Of the band systems discussed above, the $B^2\Sigma^+ - X^2\Sigma^+$ transition is idiosyncratic of the AX^+ molecular ions, while the $C^2\Pi_r - X^2\Sigma^+$ system has a well-known analog, the $A-X$ bands, in the case of the neutral MX molecules. However, there is another important excited state of MX, the $B^2\Sigma^+$, with its well-known $B-X$ emission bands, observed in many MX molecules. Both the MX $A^2\Pi$ and the $B^2\Sigma^+$ state are ionically bound. The corresponding states should also exist in the AX^+ case. The first of these, $\text{AX}^+ C^2\Pi_r$, has been discussed above. The $B^2\Sigma^+$ state of MX should then also have an AX^+ analog with similar properties. It should here be termed $D^2\Sigma^+$. Like the $C^2\Pi_r$ state, it will correlate diabatically with the $\text{A}^{++}(^2P) + \text{X}^-$ asymptote (see Fig. 2), but adiabatically, as a result of avoided crossings, with the $\text{A}^+(^3P) + \text{X}$ level. For clarity, only the latter portion of the D state potential has been indicated in Fig. 2, while its well, expected to be close to that of $C^2\Pi_r$, and the Coulombic portion have been omitted.

Some of the features observed in our spectra may in fact be due to the expected $D^2\Sigma^+ - X^2\Sigma^+$ transitions, corresponding to the $B-X$ bands of MX. In the $\text{Ga}^+ + \text{Cl}_2$, $\text{Ga}^+ + \text{Br}_2$, and $\text{In}^+ + \text{Br}_2$ reactions, the emission intensity at 2500–2600 Å, around 2700, and near 2900 Å, respectively (Fig. 1), does not appear to belong to the $C-X$ band systems. This is especially clear in the latter case, in comparison with

$\text{In}^+ + \text{Cl}_2$, where no corresponding peak is seen. The same three features appear also in the high-resolution spectra, Fig. 4, as structureless humps. If these emissions are transitions to the AX^+ ground states, the compactness of the band systems indicates an upper state potential having a similar r_e as the ground state. This is consistent with the expected character of the $D^2\Sigma^+$ state, which should be ionically bound in a way much like the ground state. Also, because the AX^+ $C^2\Pi$ and $D^2\Sigma$ states both correlate diabatically to the common asymptote $\text{A}^{++}(^2P) + \text{X}^-$, it is expected that they lie energetically close together, in agreement with the $C-X$ and $D-X$ observed in this work. In contrast to the ordering of the $A^2\Pi$ and $B^2\Sigma$ states of MX , in the case of AX^+ the $^2\Pi$ state lies slightly above the $^2\Sigma^+$ state. This could be explained by a slight upward shift of the $C^2\Pi_i$ state as a result of quantum mechanical "repulsion" by the lower-lying $A^2\Pi_i$ state (cf. Fig. 2), which might easily raise the C state above the $D^2\Sigma^+$ level. For $\text{MX}(B^2\Pi)$, there is no such repulsion by a lower $^2\Pi$ state. In InCl^+ we do not observe the proposed $D-X$ emission feature. It may here be hidden under the longer-wavelength component of the $C-X$ transition; in GaCl^+ it also appears only as a shoulder.

For AlF^+ , very recent *ab initio* results³¹ show a $D^2\Sigma^+$ state which is bound, but only weakly with respect to the $\text{Al}^+(^3P) + \text{F}$ asymptote. The same work gave a $C^2\Pi$ state below the $D^2\Sigma^+$. This need not be in conflict, however, with the relative $C^2\Pi/D^2\Sigma^+$ ordering proposed above for the heavier Ga and In systems: In the Be and Mg halides the $^2\Sigma^+$ state lies also anomalously high above the $^2\Pi_i$ state compared to the heavier alkaline earth halides.

CONCLUSION

The systematic spectroscopic study of 12 group IIIa monohalide ions (AX^+) presented in this work has provided comprehensive information on electronically excited states in this important, but hitherto little explored class of molecules. Very extensive spectroscopic data have been obtained: In ten cases, $B^2\Sigma^+-X^2\Sigma^+$ band systems have been observed, nine of them for the first time. $C^2\Pi_i-X^2\Sigma^+$ transitions have been discovered for six AX^+ ions, four of them with resolved fine structure. Finally, in three cases newly found spectral features have been assigned to $D^2\Sigma^+-X^2\Sigma^+$ band systems, transitions which are very well known in the isoelectronic alkaline earth halides MX , but have never been reported on in the literature, including theoretical, for AX^+ . Combining this wealth of new spectroscopic information with results from photoelectron spectroscopy, some *ab initio* calculations, the—very sparse—previous optical observations, and data on the MX spectroscopy, we have been able to obtain clear insight into the electronic structure of the AX^+ species. This section summarizes our present understanding of the electronic states of AX^+ in terms of their leading electron configurations.

Figure 6 illustrates diagrammatically, for the specific example of AlF^+ , the occupancy of the valence molecular orbitals and the corresponding character of the bonding. The parent AlF ground state, $^1\Sigma^+$, is essentially ionically bound, dissociating adiabatically to $\text{Al}^+(3s^2) + \text{F}^-(2p^6)$

Species	Symmetry	Configuration						Character
		No.	6σ	2π	7σ	8σ	3π	
AlF^+	$^2\Pi_i$	⑨	•	•••••	•		•	$(\text{Al}^+)^* \text{F}$
	$^2\Sigma^+$	⑧	•	•••••	•	•		$(\text{Al}^+)^* \text{F}$
	$^2\Sigma^+$	⑦	•	•••••	•		•	$(\text{Al}^+)^* \text{F}$
	$^2\Pi_i$	⑥	•	•••••	•	•		$(\text{Al}^+)^* \text{F}$
	$^2\Pi_i$	⑤	•	•••••			•	$(\text{Al}^+)^* \text{F}^-$
	$^2\Sigma^+$	④	•	•••••		•		$(\text{Al}^+)^* \text{F}^-$
	$^2\Sigma^+$	③	•	•••••	•••••			$\text{Al}^+ \text{F}$
	$^2\Pi_i$	②	•	•••••	•••••			$\text{Al}^+ \text{F}$
	$^2\Sigma^+$	①	•	•••••	•••••			$\text{Al}^{++} \text{F}^-$
AlF	$^1\Sigma^+$	⑩	•••••	•••••	•••••			$\text{Al}^+ \text{F}^-$

FIG. 6. Electronic configurations and state symmetries of the AX^+ molecular ions considered in this work, exemplified by AlF^+ . Five orbitals (6σ through 3π) are included, and their principal atomic orbital parentage is indicated at the bottom. The bonding character (predominantly ionic, $\text{Al}^{++} \text{F}^-$, or covalent, $\text{Al}^+ \text{F}$) is also shown.

(configuration "0"). As has been discussed very succinctly by Berkowitz and Dehmer⁵ for the general class of AX molecules, the outermost σ MO is largely an s orbital on the A atom, in our case an $\text{Al } 3s$ electron. Its removal, in the formation of AlF^+ , configuration 1, produces therefore an $\text{Al}^{++} \text{F}^-$ structure with increased ionic character. Ejection of an electron from the $\text{F}^-(2p)$ shell, on the other hand (configurations 2 and 3) leads to an $\text{Al}^+ \text{F}$ structure, thus effectively destroying the ionic bond.⁵ If, in the first case, the ionization is accompanied by a promotion of the remaining $\text{Al } 3s$ electron to $\text{Al } 3p$ (configurations 4 and 5), a strongly ionically bound structure $(\text{Al}^{++})^* \text{F}^-$ is generated, correlating with the 2P state of the (alkali-like) Al^{++} . Finally, configurations 6–9 correspond to ionization out of the $\text{F}(2p^6)$ shell with simultaneous $\text{Al}(3s \rightarrow 3p)$ excitation, correlating with the 3P state of Al^+ .

Referring now to Table VIII and Fig. 2, the observed electronic AX^+ states can be described in terms of the electron configurations listed in Fig. 6. As a result of the avoided crossings discussed above most of these adiabatic states change their character as the internuclear distance r is varied. The ground state $X^2\Sigma^+$, following the view expressed in Ref. 5, is ionically bound at short and medium distances, but correlates adiabatically to ground state $\text{A}^+(^1S) + \text{X}(^2P)$, thereby changing to the (σ -type) configuration 3. The $A^2\Pi_i$

TABLE VIII. Principal configurations of the lowest AX^+ electronic states.^a

State	Range of internuclear distance		
	Short	Medium	Long
$X^2\Sigma^+$	1	1	3
$A^2\Pi_i$	2	2	2
$B^2\Sigma^+$	3	1	8
$C^2\Pi_i$	5	5	9
$D^2\Sigma^+$	4	?	7
$E^2\Pi_i$?	?	6

^aFor key to the configuration numbering, see Fig. 6.

state has the asymptotically identical, but Π -type configuration 2 at all distances. As expected from simple electron cloud overlap pictures, it is, therefore, repulsive. The B state reveals at small r its origin, via an avoided crossing, from the same $A^+(^1S) + X(^2P)$ asymptote (configuration 3). At medium r it will take over the ionic character (configuration 1) from the ground state diabatic correlation. Finally, however, the B state connects with the excited $A^+(^3P) + X$ asymptote. Here, of the two configurations compatible with a $^2\Sigma^+$ state, configurations 7 and 8, only the latter will give the required covalent bonding between the $F(2p\sigma)$ and the $Al(3p\sigma)$ orbital. The important $C^2\Pi_r$ state, from the discussion given above, will have mainly $A^{++}(^2P) + X^-$ character in the bonding region, corresponding to configuration 5. It dissociates, however, to $A^+(^3P) + X$, having, from Fig. 6, $^2\Pi$ configurations 6 or 9. Again, only one of these, configuration 9, will give covalent bonding. Configuration 6 will exhibit repulsion of the doubly occupied $F(2p\sigma)$ orbital, and is expected to give rise to an unbound $^2\Pi_i$ state ("E" in Fig. 2). Lastly, configuration 7 will also give a long-range repulsive state from the same asymptote of $^2\Sigma^+$ symmetry. It will, however, connect to the bound $D^2\Sigma^+$ state, which has been discussed above to be ionically bound. This state is, therefore, at small r expected to have principally the configuration 4.

The qualitative arguments presented here are by no means purely speculative. At least in the case of AlF^+ , they are supported quantitatively by a preliminary MCSCF-CI calculation.³¹ The configuration analysis of the computed wave functions conforms in every detail to the intuitive expectation.

ACKNOWLEDGMENTS

We thank the Deutsche Forschungsgemeinschaft for the funds to purchase the photon detector used in this work. One of us (A.K.) thanks the Alexander von Humboldt foundation for a fellowship. We are indebted to Professor C. A. de Lange and Dr. O. Grabandt, Amsterdam, and Dr. J. Migdalek, Krakow, for making unpublished results available to us. We are especially grateful to Dr. R. Klein, Dr. P.

Knowles, Dr. P. Rosmus, Dr. J. Senekowitsch, and Professor H.-J. Werner for inviting one of us (B.M.) to cooperate with preliminary *ab initio* calculations and for communicating results prior to publication.

APPENDIX

Here we wish to comment on the additional spectral features appearing in Fig. 1. These are of four different types:

Atomic lines from B(I), Al(I), Ga(I), In(I)

The principal lines are listed in Table IX. It is seen that most of them are due to the resonance transitions from the n^2S and n^2D states to the atomic ground states, n^2P ($n = 2-5$ for B-In). In the case of $Al^+ + Cl_2, Br_2$, higher members of the $^2S, ^2D \rightarrow ^2P$ Rydberg series are also seen at short wavelengths. For collisions of B^+ with H_2 and other simple gases the analogous luminescent charge transfer has been thoroughly studied.³⁴ It was found that direct electron capture by the projectile ion from the target gas (luminescent charge transfer) is only important at high collision energies. A residual emission at energies below the thermodynamic threshold was shown to be due to charge transfer occurring outside the collision chamber, prior to the ion deceleration, with background target gas; the resulting fast, neutralized projectile particles were then collisionally excited in the target gas cell to give the observed emission. In the present work this two-step mechanism is also very likely responsible for most of the atomic lines observed. For metastable $A^+(^3P)$ ions, the threshold energies given in Table X are in many cases accessible at the energies to which Fig. 1 refers (cf. Table I). Additional spectra taken with Al^+ at much lower energies, however, confirm that the two-step mechanism is nevertheless operative at least for this ion. Only for the Ga lines shown in Fig. 1 we cannot exclude a contribution from direct luminescent charge transfer occurring within the cell.

The relative intensities of these atomic emissions increase in the order $F_2-Cl_2-Br_2$, as can be qualitatively seen in the Al^+ panels of Fig. 1 (where the three plot scales are very roughly comparable). This is consistent with the decreasing ionization potentials $IP(X_2)$ of 15.69, 11.50, 10.52 eV,

TABLE IX. Wavelengths of observed atomic lines (in Å) and valence electron quantum numbers in the upper state.^a

Boron		Aluminum		Gallium		Indium	
B I	$3s'$ 2497;2498 $2p^2$ 2089;2090	Al I	$4s'$ 3962;3944 $5s'$ 2652;2660 $6s'$ 2372;2378 $7s'$ 2258;2264 $8s'$ 2199;2205 $3d$ 3092;3082 $4d$ 2568;2575 $5d$ 2367;2373 $6d$ 2263;2269 $7d$ 2205;2210 $8d$ 2169;2174	Ga I	$5s'$ 4172 $6s'$ 2720 $4d$ 2944;2874 $5d$ 2500;2450 $6d$ 2338	In I	$6s'$ 4511 $5d$ 3039;3256 $5p$ 2307
B II	$2p^2 \rightarrow 2p$ 4122 $4f \rightarrow 3d$ 3451	Al II	$3p$ 2670	Ga II	$4p$ 2091		

^a The lower state is the ground state in all cases except B II, where it is indicated separately. Identification based on Refs. 2, 32, and 33.

TABLE X. Endothermicities of neutral excited product channels^a (in eV).

System	Product	
	A ^{*b}	AX*(A ¹ Π)
A ⁺ (³ P) + X ₂		
B ⁺ + F ₂	7.8–8.8	4.6
Cl ₂	3.6–4.6	1.7
Br ₂	2.6–3.4	0.6
Al ⁺ + F ₂	8.2–9.1	7.5
Cl ₂	4.0–6.5	4.6
Br ₂	3.0–5.5	3.5
Ga ⁺ + F ₂	6.7	6.8
Cl ₂	2.5–4.9	3.6
Br ₂	1.5–3.9	2.0
In ⁺ + F ₂	7.3	7.8
Cl ₂	3.1–4.1	4.6
Br ₂	2.0–3.0	3.2

^aMolecular data from Ref. 3 and Table III, atomic data from Ref. 17.

^bThe range of energies given corresponds to the lowest and the highest product states observed in this work.

which would tend to give an increasing cross section for the neutralization step $A^+(^1S, ^3P) + X_2 \rightarrow A(^2P) (\text{fast}) + X_2^+$.

Atomic lines from B⁺, Al⁺, Ga⁺, In⁺

These background lines appearing in the Al⁺, Ga⁺, and In⁺ spectra of Fig. 1 are the AlII(³P₁–¹S₀) intercombination lines, at 2670, 2091, 2307 Å, respectively. The corresponding upper state lifetimes are 300,³⁵ 5.3,³⁶ and ~0.13 μs.³⁷ Thus for Al⁺ and Ga⁺, ions formed in the ³P₁ state in the ion source will survive the time of flight to the target cell (10–20 μs) and are detected directly. In⁺(³P₁), however, will radiatively decay before reaching the observation zone. Here the observed emission is ascribed to radiative cascades from a long-lived precursor or to collision-induced intramultiplet mixing $In^+(^3P_{0,2}) + X_2 \rightarrow In^+(^3P_1) + X_2$ from the very long-lived ³P_{0,2} components, which are also present in the A⁺ beams.

In the case of Al⁺ it was directly verified that the emission line also appeared without collision gas in the cell, consistent with the above interpretation. The intensity of this line, together with the absolutely known transition probability, can be used to derive absolute chemiluminescence cross sections in an elegant way.¹¹ For B⁺, the ³P₁–¹S₀ intercombination transition has a lifetime of 0.1 s, and the corresponding line at 2678 Å does therefore not appear. The two BII lines, shown in Fig. 1, at 4122 Å and (very weak) at 3451 Å, are probably observable on account of long-lived precursor transitions (especially the first, which is due to a transition not far from the ionization limit).

Cl₂⁺ and Br₂⁺ emission

In the boron panel of Fig. 1, the extensive band systems Cl₂⁺, Br₂⁺(A²Π_u–X²Π_g) are marked. They were identified from data given in Refs. 3 and 16 and are due to luminescent charge transfer $B^+ + Cl_2, Br_2 \rightarrow B + Cl_2^+(A), Br_2^+(A)$. This process is endothermic by 5.65 eV (4.75 eV) for ground state B⁺ on Cl₂(Br₂) and by 1.02 (0.12) eV for metastable B⁺ ions. Thus, at the collision energies used, metastable

B⁺(³P) is most likely responsible for the observed emission. With F₂ even B⁺(³P) has a threshold energy of 5.56 eV for the excitation of F₂⁺(A²Π_u), while the spectrum in Fig. 1 was taken at a collision energy of 3.9 eV_{CM}. Consequently no F₂⁺ emission at 4220–5090 Å¹⁶ is observed here.

Chemiluminescence giving neutral AX* product

Besides chemiluminescent reactions of the type of Eq. (1), giving excited molecular ions AX⁺, the formation of AX* + X⁺ products can also occur. For the systems considered here these channels are all fairly endothermic. The threshold energies for metastable A⁺(³P) reactants are given in the last column of Table X [ground state A⁺(¹S) ions cannot react at the collision energies listed in Table I]. There is, in fact, some evidence for reactions of this type in our spectra.

In Fig. 1 two weak emissions are shown which are due to the BCl and BBr A¹Π–X¹Σ⁺ transitions.³ Spectra taken of these features at 6 Å resolution revealed very clearly sequences of the known BCl and BBr bands. These emitters are formed in the chemiluminescent ion–molecule reactions $B^+ + X_2 \rightarrow BX^* + X^+$. Interestingly, these are the two least endothermic reactions among those listed in Table X. Pending a confirmation of the bimolecular reaction mechanism by a measurement of the light yield as a function of X₂ pressure, these reactions have here been observed for the first time. A separate study of their dynamics would be of interest, in particular in comparison with the chemiluminescence of the isoelectronic species CCl⁺(A¹Π), which has been observed in preliminary experiments on C⁺ + Cl₂ and C⁺ + HCl collisions.³⁸ A possible contribution from the AlBr(A¹Π–X¹Σ⁺) transition to the emission observed with Al⁺ + Br₂ near 2790 Å has been commented on above. Finally, the three features marked with an asterisk in Fig. 1 coincide with the C–X band systems of GaCl, GaBr, and InBr, again the lowest ¹Π–¹Σ transition like in BCl and BBr. They could, therefore, also be due to the corresponding A⁺ + X₂ → AX* + X⁺ reactions, an alternative to the explanation as AX⁺(D²Σ⁺–X²Σ⁺) transitions given above. However, unlike the spectroscopically well characterized BCl and BBr ¹Π states, with GaCl, GaBr, and InBr the corresponding states are very weakly bound and predissociated, and have never been observed in emission (except for a remark in Ref. 39). It is therefore somewhat improbable that we should see such distinct emission features from those species. Furthermore, InCl ¹Π–¹Σ⁺ emission, which has been observed at 2670–2740 Å,⁴⁰ would then also be expected, but is clearly absent (Figs. 1 and 4). Finally, a simple rule, based on relative ionization potentials,⁴¹ predicts dominance of the reaction channel $A^+ + X_2 \rightarrow AX^{++} + X$ over the competing formation of AX* + X⁺. For all these reasons, we favor an interpretation of the three emission features as given in the text.

¹Emission Spectroscopy, edited by R. M. Barnes (Halsted, New York, 1976).

²W. Grotrian, *Graphische Darstellung der Spektren von Atomen und Ionen mit ein, zwei, und drei Valenzelektronen* (Springer, Berlin, 1928), Vols. 1 and 2.

³K. P. Huber, G. Herzberg, *Molecular Spectra and Molecular Structure*,

- IV. *Constants of Diatomic Molecules* (Van Nostrand, New York, 1979).
- ⁴J. M. Dyke, C. Kirby, and A. Morris, *J. Chem. Soc. Faraday Trans. 2* **79**, 483 (1983).
- ⁵J. Berkowitz and J. L. Dehmer, *J. Chem. Phys.* **57**, 3194 (1972).
- ⁶R. G. Egdell and A. F. Orchard, *J. Chem. Soc. Faraday Trans. 2* **74**, 1179 (1978).
- ⁷J. M. Dyke, C. Kirby, A. Morris, B. W. J. Gravenor, R. Klein, and P. Rosmus, *Chem. Phys.* **88**, 289 (1984).
- ⁸W. J. Balfour and K. S. Chandrasekhar, *J. Mol. Spectrosc.* **124**, 443 (1987).
- ⁹S. Yamaguchi, M. Tsuji, and Y. Nishimura, *Chem. Phys. Lett.* **138**, 29 (1987).
- ¹⁰M. Menzinger, in *Gas Phase Chemiluminescence and Chemi-Ionization*, edited by A. Fontijn (Elsevier, New York, 1985).
- ¹¹A. Kowalski, B. Müller, and Ch. Ottinger, *Chem. Phys.* (in press).
- ¹²R. V. Hodges, P. B. Armentrout, and J. L. Beauchamp, *Int. J. Mass Spectrom. Ion Phys.* **29**, 375 (1979).
- ¹³Ch. Ottinger, in *Gas Phase Ion Chemistry*, edited by M. T. Bowers (Academic, New York, 1984), Vol. 3, p. 249.
- ¹⁴J. Reichmuth, *Diplomarbeit, Max-Planck-Institut für Strömungsforschung* (Göttingen, 1981).
- ¹⁵Ch. Ottinger and J. Reichmuth, *J. Chem. Phys.* **74**, 928 (1981).
- ¹⁶R. W. B. Pearse and A. G. Gaydon, *The Identification of Molecular Spectra* (Chapman and Hall, London, 1976).
- ¹⁷C. E. Moore, *Atomic Energy Levels*, Natl. Bur. Stand. Ref. Data Ser. Natl. Bur. Stand. 35 (U.S. GPO, Washington, D.C., 1971).
- ¹⁸*CRC Handbook of Chemistry and Physics*, 58th ed., edited by R. C. Weast (CRC, West Palm Beach, 1977).
- ¹⁹R. Klein, P. Rosmus, and H. J. Werner, *J. Chem. Phys.* **77**, 3559 (1982).
- ²⁰B. Müller and Ch. Ottinger, *J. Chem. Phys.* **85**, 232 (1986).
- ²¹J. Berkowitz, *J. Chem. Phys.* **56**, 2766 (1972).
- ²²E. U. Condon, *Phys. Rev.* **32**, 858 (1928); D. J. Ehrlich and R. M. Osgood, Jr., *Phys. Rev. Lett.* **41**, 547 (1978); D. Eisel, D. Zevgolits, and W. Demtröder, *J. Chem. Phys.* **71**, 2005 (1979).
- ²³P. Rosmus (private communication).
- ²⁴O. Grabandt and C. A. de Lange (private communication).
- ²⁵C. Nelin, B. O. Roos, and A. J. Sadlej, *J. Chem. Phys.* **77**, 3607 (1982).
- ²⁶G. H. F. Diercksen and A. J. Sadlej, *Chem. Phys. Lett.* **84**, 390 (1981).
- ²⁷This value was assumed, considering experimental results of H. Cooker, *J. Phys. Chem.* **80**, 2078 (1976) and a critical discussion of the results in Ref. 26.
- ²⁸The lowest excited state of M^+ is 2P only for the cases of Be^+ and Mg^+ . For Ca^+ , Sr^+ , Ba^+ the lowest excited state is 2D which lies 1.4, 1.2, 1.9 eV below the respective 2P level (Ref. 17). In these cases the $MXA^2\Pi$ states correlate therefore adiabatically with $M^+(^2D) + X^-$. Nevertheless, the contribution of $M^+(^2P)$ to the $MX(^2\Pi)$ wave function at r_c is still very considerable. For $M = Ca$, it has been calculated to be 69%, 62%, 60%, and 55% for $X = F, Cl, Br, I$, respectively (Ref. 29).
- ²⁹S. F. Rice, H. Martin, and R. W. Field, *J. Chem. Phys.* **82**, 5023 (1985).
- ³⁰Note that for all A^{++} ions considered here, the lowest excited state is 2P , while the 2D state lies much higher (Ref. 17). Thus, the contribution of $A^{++}(^2P)$ to the $AX^+C^2\Pi$ state should be much greater than that of $M^+(^2P)$ in the analogous $A^2\Pi$ states of MX (Ref. 28).
- ³¹P. Knowles, B. Müller, Ch. Ottinger, P. Rosmus, J. Senekowitsch, and M. J. Werner (to be published).
- ³²A. R. Striganov and N. S. Sventitskii, *Tables of Spectral Lines of Neutral and Ionized Atoms* (IFI/Plenum, Washington, 1968).
- ³³S. Bashkin and J. O. Stoner, Jr., *Atomic Energy Levels and Grotrian Diagrams* (North-Holland, New York, 1975).
- ³⁴Ch. Ottinger, J. Reichmuth, and M. Yang, *Chem. Phys.* **76**, 61 (1983).
- ³⁵B. C. Johnson, P. L. Smith, and W. H. Parkinson, *Astrophys. J.* **308**, 1013 (1986).
- ³⁶J. Migdalek (private communication).
- ³⁷T. Andersen and G. Sørensen, *Phys. Rev. A* **5**, 2447 (1972).
- ³⁸Th. Glenewinkel-Meyer, H. Tischer, and Ch. Ottinger (unpublished results).
- ³⁹V. Singh, A. Rai, S. Rai, and D. Rai, *J. Phys. B* **20**, L45 (1987).
- ⁴⁰K. Perumalsamy, S. B. Rai, K. N. Upadhyay, and D. K. Rai, *Physica C* **132**, 122 (1985).
- ⁴¹Ch. Ottinger, in *Gas-Phase Chemiluminescence and Chemi-Ionization*, edited by A. Fontijn (Elsevier, New York, 1985), p. 117.